

Article

Humidity Controlled Mechanical Properties of Electrospun Polyvinylidene Fluoride (PVDF) Fibers

Piotr K. Szewczyk , Daniel P. Ura  and Urszula Stachewicz * 

International Centre of Electron Microscopy for Materials Science, Faculty of Metals Engineering and Industrial Computer Science, AGH University of Science and Technology, Al. A. Mickiewicza 30, 30-059 Kraków, Poland; pszew@agh.edu.pl (P.K.S.); urad@agh.edu.pl (D.P.U.)

* Correspondence: ustachew@agh.edu.pl

Received: 28 September 2020; Accepted: 14 October 2020; Published: 16 October 2020



Abstract: Processing parameters in electrospinning allow us to control the properties of fibers on a molecular level and are able to tailor them for specific applications. In this study, we investigate how relative humidity (RH) affects the mechanical properties of electrospun polyvinylidene fluoride (PVDF). The mechanical properties of single fibers were carried out using a specialized tensile stage. The results from tensile tests were additionally correlated with high-resolution imaging showing the behavior of individual fibers under tensile stress. The mechanical characteristic is strongly dependent on the crystallinity, chain orientation, and fiber diameter of electrospun PVDF fibers. Our results show the importance of controlling RH during electrospinning as the mechanical properties are significantly affected. At low RH = 30% PVDF fibers are 400% stiffer than their counterparts prepared at high RH = 60%. Moreover, the vast differences in the strain at failure were observed, namely 310% compared to 75% for 60% and 30% RH, respectively. Our results prove that humidity is a crucial parameter in electrospinning able to control the mechanical properties of polymer fibers.

Keywords: PVDF; mechanical properties; humidity; electrospinning; tensile testing

1. Introduction

Many applications of electrospun polymer fibers depend greatly on their mechanical properties, which are governed by processing conditions in electrospinning [1–3]. With the right set of parameters, we are able to obtain a broad range of morphologies and physicochemical properties from the same raw material [2,4–6]. Thus far, electrospun fibers have been researched in a wide variety of applications such as cost-effective water harvesting systems [7,8], energy harvesters [9–11], tissue engineering scaffolds [12,13], filters [14–16], composite strengtheners [17–19], sensors [20], drug delivery systems [21,22] and many more.

Characterization of mechanical properties of single polymer fibers is difficult due to often micro- and nanosized dimensions of the samples, making the handling and testing challenging [23]. There are many reports on fiber meshes that were measured using macroscale experimental methods [23–26]. Such an approach gives important information on how electrospun membranes behave under load together with a few proposed models of stretched electrospun samples [27]. Importantly, there are many parameters in electrospinning and all of them affect the properties of produced fibers [28,29]. One of them is relative humidity (RH) [30]. Humidity influences fiber diameters [31], crystallinity [32], internal structure [33], surface roughness [34], and mechanical properties of electrospun fibers [30,35,36]. Recent reports have shown that key properties such as stiffness, strain at break, or Young's modulus can be controlled using just RH [30,35,36]. The importance of RH is often correlated with the phase separation processes that take place in a humid atmosphere. Vapor-induced phase separation (VIPS) is frequently proposed as the main mechanism of phase separation in the electrospinning process. In this

phenomenon, humid air condenses on polymer jet mid-flight leading to changes in morphology and porosity as well as affect the structure of obtained fibers [37,38].

In this study, we investigate how RH affects the mechanical properties of polyvinylidene fluoride (PVDF), which has a broad range of applications due to its high mechanical strength, chemical resilience, biocompatibility, and piezoelectric properties [39–41]. As a result of those properties, PVDF can be found in applications from tissue engineering to water and energy harvesting [8,32,42], where controlled mechanical properties of fibers are highly desirable [43]. Thus, we focus in this paper on the mechanical properties of PVDF fibers electrospun at low (30%) and high (60%) RH. To fully understand how processing parameters affect the properties of electrospun fibers, testing of individual fibers was performed. Detailed investigation of individual fibers under stress was carried out utilizing in-situ tensile testing in scanning electron microscope (SEM). Additionally, the mechanical properties were discussed with the crystallinity values for similar samples. This work shows the strong influence of RH on the morphology and mechanical properties of individual electrospun PVDF fibers.

2. Materials and Methods

2.1. Electrospinning

PVDF ($M_w = 275,000 \text{ g mol}^{-1}$, Sigma Aldrich, London, UK) 24 wt.% was dissolved in acetone (analytical standard, Avantor, Gliwice, Poland) and dimethylacetamide (DMAC, analytical standard, Avantor, Gliwice, Poland) in a 1:1 ratio. The PVDF solution was stirred for 4 h at a constant speed of 700 rpm on a hot plate set to 55 °C (IKA RCT basic, Staufen, Germany). The solution was electrospun using EC-DIG (IME Technologies, Waalre, The Netherlands) apparatus with a climate upgrade system. A constant voltage of 15 kV was applied to the stainless-steel needle with an inner diameter of 0.8 mm situated at a 14 cm distance from the collector. The flow rate of the solution for all samples was set to 4 mL·h⁻¹. Ambient temperature was kept constant at $T = 25 \text{ °C}$ and the RH was set to 30 or 60%. In this study, the samples are labeled as PVDF30 and PVDF60 for their respective RH. To obtain the aligned fibers the rotating collector at 2500 rpm was used to deposit fibers for 5 s on custom-made frames with a 3 × 3 mm window.

2.2. Mechanical Testing and Microscopy

Mechanical testing was carried out using a tensile module equipped with a 1N (load resolution $1 \times 10^{-5} \text{ N}$) load cell (B.1708.A, Kammrath & Weiss, Dortmund, Germany) using 20 $\mu\text{m s}^{-1}$ extension rates, see the image of the tensile stage in the Supplementary Materials, Figure S1. The tests were performed at $T = 24 \text{ °C}$ and RH = 50%. The average values of the maximum strength (σ_{max}), toughness (W), Young's modulus (E), strain at maximum stress (ε_{max}), and strain at failure (ε_f) were calculated from three separate measurements. Young's modulus was calculated based on linear fitting in 0.5 to 1% strain region. In Figure 1, the experimental set-up is presented. The movie of tensile tested single PVDF fibers is available the Supplementary Materials (Tensile_test_single_fiber_PVDF60).

The mechanical testing was performed also in-situ in SEM to investigate the deformation of individual fibers. Prior to SEM imaging, samples were covered from both sides with a 10 nm layer of Au using a rotary sputter coater (Quorum, Lewes, UK) to ensure conductivity and act as a contrast to non-coated sections of polymer fibers exposed with elongation. The imaging of PVDF during testing was performed using an accelerating voltage of 2.5 kV at a working distance of 11–13 mm. To image the cross-sections, the PVDF fibers were freeze-fractured using LN₂ (Figure 1). After fracturing, the samples were prepared and imaged at the same setting as during the tensile testing. The diameters of PVDF30 and PVDF60 fibers were taken as an average of 100 fibers calculated from SEM images. The mechanical testing for stress-strain characteristics showed in Figure 2 were carried out in ambient conditions outside SEM to avoid any beam effect on the collected results [44]. All data were analyzed using OriginPro (v2019 SR1, OriginLab, Northampton, MA, USA) software. Stress-strain curves were

smoothed using the second polynomial order Savitzky-Golay filter with 512 points of window; see Figure S2 in the Supplementary Materials for the raw data of load-displacement curves.

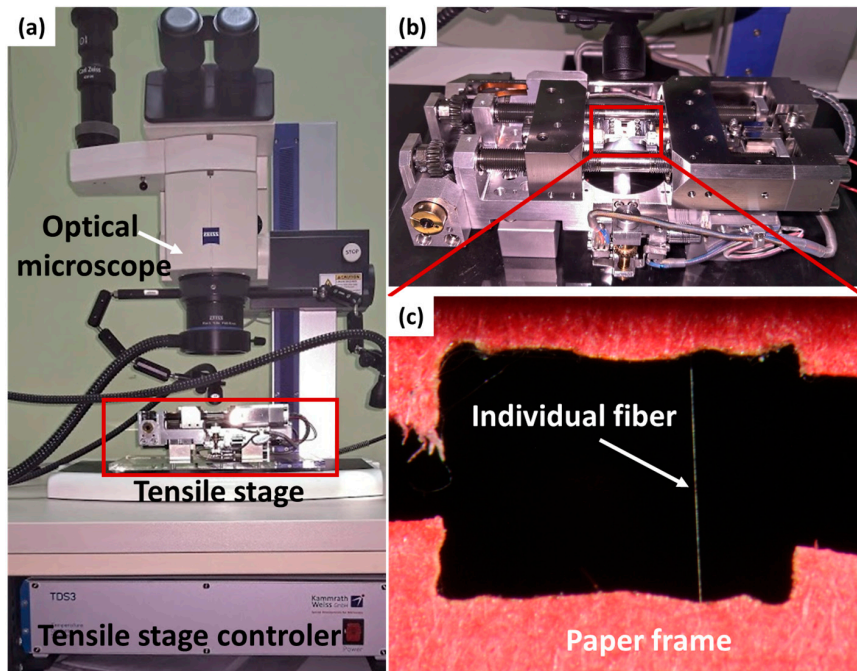


Figure 1. Experimental set-up for the tensile testing. (a) Macrophotography of tensile stage placed under the microscope, (b) tensile stage with a mounted sample, (c) sample image of PVDF fiber located in the frame.

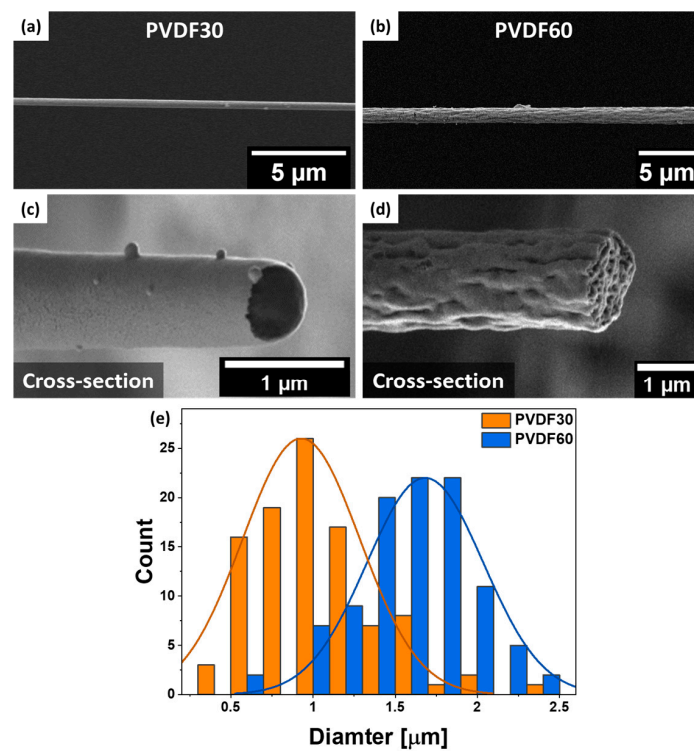


Figure 2. SEM images of initial morphology and cross-sections from PVDF electrospun at (a,c) 30 and (b,d) 60% RH, respectively and (e) distribution of fiber diameters as measured from SEM images.

Toughness was calculated as a function of area under the curve using OriginPro using integrate function which is based on a given equation:

$$\int_0^b f(x)dx, \quad (1)$$

where b = strain at failure, $f(x)$ = stress and x = strain. Strain at the maximum stress was calculated as strain value in the maximum height of the stress-strain curve and tensile strength was given as the maximum value of stress. Both calculations were carried out using the integrated function in OriginPro. The error was based on the standard deviation.

3. Results and Discussion

SEM observation revealed smooth surfaces with a solid core for PVDF30 fibers, while, conversely, PVDF60 fibers had distinct wrinkled surfaces and exhibited internal porosity; see Figure 2. The average fiber diameters were $0.92 \pm 0.36 \mu\text{m}$ and $1.68 \pm 0.35 \mu\text{m}$ for PVDF30 and PVDF60, respectively; see histograms presented in Figure 2e. Those changes to fiber morphology and average diameter were driven by humidity variation during electrospinning and vapor affecting PVDF fibers. This is an excellent example of VIPS, where water vapor present in the humid air causes polymer jet to separate into polymer-rich and polymer-lean phase. When the solvent is evaporated, polymer-lean phase turns into voids and the polymer-rich phase yields a solid material [45]. Importantly, for this process to occur, high amounts of water vapor are necessary; therefore, VIPS process only occurred for RH of 60%. For PVDF30 the RH was too low to initiate phase separation which led to smooth and solid fibers [32].

In Figure 3, we present the stress-strain curves from the tensile testing of single PVDF fibers carried out in ambient conditions. Multiple upper and lower yield points on all obtained curves indicate that numerous necks appear on stretched fibers which correlates well with in-situ observations [46]. We observed that fibers with both unstretched regions and necks indicated on SEM micrographs of individually tested fibers, see Figure 3b,c. The necking behavior that we show is typical for the deformation of semi-crystalline polymers, which is caused by a transition from lamellar to a fibrillar structure [46–48]. In this transition, originally crystalline portions of the material are deformed by stress into fibrils. Such behavior is caused by stress concentrated on the surface of the lamellar crystals, which promotes localized crystal slip and fragmentation [49].

In Table 1, the summary of mechanical properties of PVDF fibers electrospun at low and high humidity are presented. PVDF60 fibers exhibited more than four times higher strain at failure, toughness and strain at maximum stress compared to PVDF30. Interestingly, both types of fibers had almost the same tensile strength of 159.2 ± 41.1 and 156.3 ± 35.6 Mpa for PVDF30 and PVDF60, respectively. Increased RH led to PVDF60 fibers with significantly lower Young's modulus of 13.3 ± 4.3 MPa compared to 3.5 ± 1.2 MPa for PVDF30. Relatively high Young's modulus of PVDF30 fibers was the result of enhanced chain slip and a smaller number of defects associated with lower fiber diameters combined with higher crystallinity [23,50–54]. Lim et al. [55] has shown that electrospun PCL fibers with smaller diameters possess a higher degree of molecular orientation and crystallinity, which makes them superior in stiffness and tensile strength at a cost of the lower ductility. Those data are in line with our findings on electrospun PVDF. As observed from Figure 3a, fibers obtained at high RH underwent plastic deformation and reached strains as high as 225%, which resulted in a high toughness. The increase in toughness between PVDF30 and PVDF60 was caused by increased chain mobility due to a lower degree of crystallinity. This difference led to much more ductile PVDF60 fibers, which underwent extensive and energy-absorbing necking prior to failure, which was made possible by chain reorientation inside of the fibers under stress [26]. Notably, for PVDF30, we also observed fluctuations in stress value—see Figure 3—that are associated with the fibers' necking. Prior to necking, the stress rises sharply, and while necking it slowly decreases. In our case, more than one neck appeared for a single fiber as seen from the stress-strain curve and SEM. This behavior was confirmed with in-situ SEM observation where we observed a higher amount of necks appearing on

the individual PVDF60 fibers when compared to PVDF30 samples. A similar behavior was reported on electrospun polyacrylonitrile (PAN) and polymethyl methacrylate (PMMA) fibers [26,56].

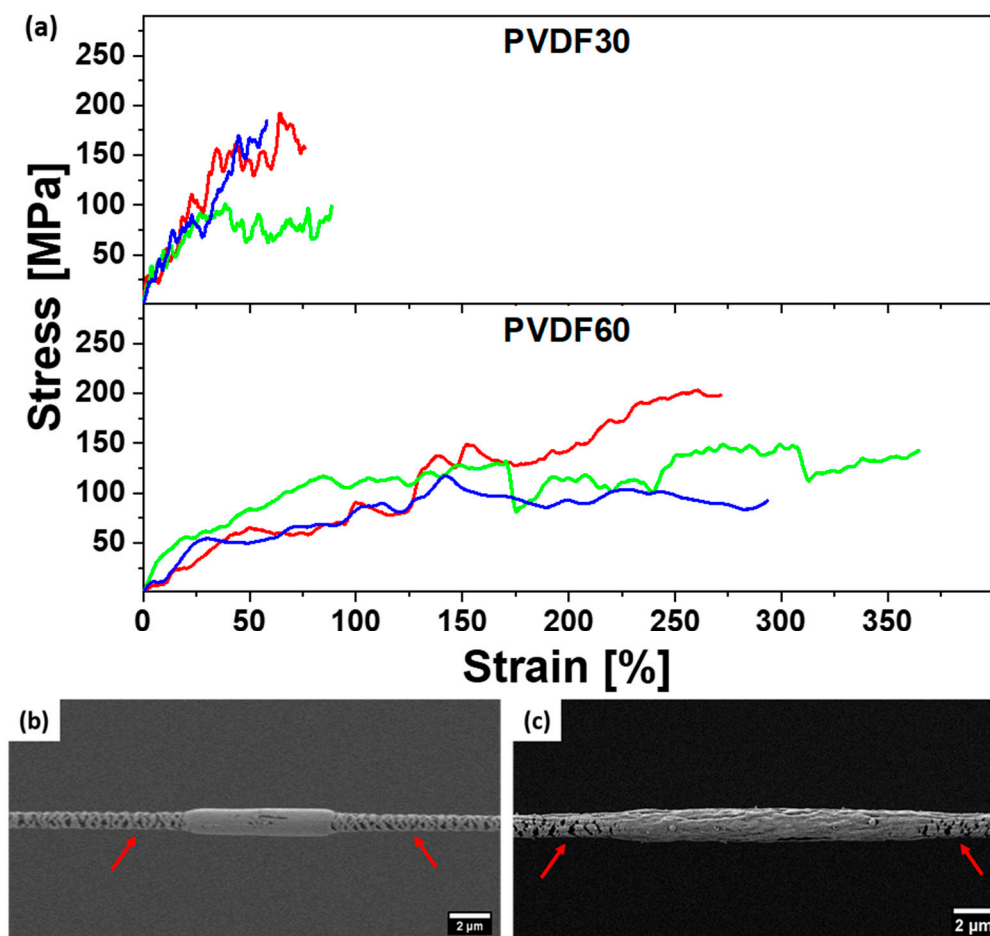


Figure 3. (a) Stress-strain curves of single PVDF fibers electrospun at RH of 30 and 60%. In-situ investigation in SEM of samples (b) PVDF30 and (c) PVDF60, with the red arrows indicating necked regions in tested fibers.

Table 1. Mechanical properties of single fibers as calculated from room condition measurements.

Sample	Strain at Failure ϵ_f [%]	Toughness W [MPa]	Tensile Strength R_m [MPa]	Strain at Maximum Stress ϵ_{max} [%]	Young's Modulus [MPa]
PVDF30	74.19 ± 12.46	69.83 ± 13.94	159.2 ± 41.1	53.64 ± 10.96	13.3 ± 4.3
PVDF60	309.89 ± 39.74	312.11 ± 70.74	156.3 ± 35.6	225.08 ± 58.93	3.5 ± 1.2

In our previous study, we reported that the overall crystallinity was $40.7 \pm 0.7\%$ and $34.1 \pm 0.2\%$ for randomly aligned PVDF30 and PVDF60, respectively [32]. Notable, those results are probably lowered as electrospun fiber crystallinity has been reported to be increased with the rotation speed of the collecting drum [57]. However, increase in crystallinity for PVDF30 fibers is caused by lower fiber diameter and a lack of voids in the material. Notably, Aristein et al. [51] proposed that the supramolecular structure of the amorphous phase was considered as a determining factor of fiber stiffness, which was verified on electrospun nylon 6 fibers. Overall crystallinity has a modest effect on the tensile properties of semi-crystalline electrospun fibers. Hence, our study has shown that the higher stiffness of PVDF30 fibers is caused by a more compact structure that leads to ordered molecular orientation with an additional contribution of higher overall crystallinity. Conversely, less crystalline

structure and internal voids in PVDF60 can lead to increased strain at failure, following with the toughness rise, see Table 1.

4. Conclusions

This study uncovered an extremely strong influence of water vapor on the resultant mechanical properties of single electrospun PVDF fibers. The changes in RH resulted in completely different morphologies of fibers. At RH of 30% smooth and solid fibers were produced, while 60% RH led to wrinkled morphology with internal voids. Vast differences in appearance translated to drastic changes in mechanical properties of obtained materials. Mechanical testing on single fibers uncovered that PVDF30 fibers were ~400% stiffer than their PVDF60 counterparts. Such change was caused by ordered supramolecular structure and lower diameters. Moreover, while PVDF60 fibers produced exhibited strain at failure of almost 310% compared to 75% for PVDF30. An in-situ investigation has shown that, in both cases, multiple necks appear during stretching. This difference was the result of the higher crystallinity and non-porous structure of PVDF30 fibers. Our findings clearly show the influence of relative humidity on a fundamental level, which affects the properties and morphology of electrospun PVDF fibers. Those findings can be used to steer the mechanical properties of entire fiber networks at no additional cost and minimal alterations to existing solutions.

Supplementary Materials: The following are available online at <http://www.mdpi.com/2079-6439/8/10/0065/s1>, Figure S1: Tensile stage loadout, Figure S2: Plots of raw data obtained from tensile stage for PVDF30 and PVDF60. Video S1: Tensile_test_of single_fiber_PVDF60.

Author Contributions: Conceptualization, U.S. and P.K.S.; methodology, P.K.S.; software, P.K.S.; validation, P.K.S., D.P.U. and U.S.; formal analysis, P.K.S.; investigation, P.K.S. and D.P.U.; resources, U.S.; data curation, P.K.S. and D.P.U.; writing—original draft preparation, P.K.S., U.S.; writing—review and editing, U.S.; visualization, P.K.S.; supervision, U.S.; project administration, U.S.; funding acquisition, U.S. All authors have read and agreed to the published version of the manuscript.

Funding: This research was funded by National Science Centre in Poland, within SONATA BIS 5 project. Grant number 2015/18/E/ST5/00230.

Acknowledgments: The study was supported by the infrastructure of the International Centre of Electron Microscopy for Materials Science, Krakow, Poland.

Conflicts of Interest: The authors declare no conflict of interest.

References

1. Xu, Y.; Gao, Y.; Wang, X.; Jiang, J.; Hou, J.; Li, Q. Internal Structure of Amorphous Electrospun Nanofiber: Oriented Molecular Chains. *Macromol. Mater. Eng.* **2017**, *302*, 1700054. [CrossRef]
2. Awal, A.; Sain, M.; Chowdhury, M. Preparation of cellulose-based nano-composite fibers by electrospinning and understanding the effect of processing parameters. *Compos. Part B Eng.* **2011**, *42*, 1220–1225. [CrossRef]
3. Inai, R.; Kotaki, M.; Ramakrishna, S. Structure and properties of electrospun PLLA single nanofibres. *Nanotechnology* **2005**, *16*, 208–213. [CrossRef] [PubMed]
4. Metwally, S.; Karbowniczek, J.E.; Szewczyk, P.K.; Marzec, M.M.; Gruszczyński, A.; Bernasik, A.; Stachewicz, U.; Stachewicz, U.; Gruszczyński, A.; Bernasik, A.; et al. Single-Step Approach to Tailor Surface Chemistry and Potential on Electrospun PCL Fibers for Tissue Engineering Application. *Adv. Mater. Interfaces* **2019**, *6*, 1801211. [CrossRef]
5. Ura, D.P.; Karbowniczek, J.E.; Szewczyk, P.K.; Metwally, S.; Kopyściański, M.; Stachewicz, U. Cell Integration with Electrospun PMMA Nanofibers, Microfibers, Ribbons, and Films: A Microscopy Study. *Bioengineering* **2019**, *6*, 41. [CrossRef]
6. Szewczyk, P.K.; Knapczyk-Korcza, J.; Ura, D.P.; Metwally, S.; Gruszczyński, A.; Stachewicz, U. Biomimicking wetting properties of spider web from *Linothele megatheloides* with electrospun fibers. *Mater. Lett.* **2018**, *233*, 211–214. [CrossRef]
7. Knapczyk-Korcza, J.; Ura, D.P.; Gajek, M.; Marzec, M.M.; Berent, K.; Bernasik, A.; Chiverton, J.P.; Stachewicz, U. Fiber-Based Composite Meshes with Controlled Mechanical and Wetting Properties for Water Harvesting. *ACS Appl. Mater. Interfaces* **2020**, *12*, 1665–1676. [CrossRef]

8. Knapczyk-Korczak, J.; Szewczyk, P.K.; Ura, D.P.; Bailey, R.J.; Bilotti, E.; Stachewicz, U. Improving water harvesting efficiency of fog collectors with electrospun random and aligned Polyvinylidene fluoride (PVDF) fibers. *Sustain. Mater. Technol.* **2020**, *25*, e00191. [[CrossRef](#)]
9. Busolo, T.; Ura, D.P.; Kim, S.K.; Marzec, M.M.; Bernasik, A.; Stachewicz, U.; Kar-Narayan, S. Surface potential tailoring of PMMA fibers by electrospinning for enhanced triboelectric performance. *Nano Energy* **2019**, *57*, 500–506. [[CrossRef](#)]
10. Kong, T.-H.; Lee, S.-S.; Choi, G.-J.; Park, I.-K. Churros-like Polyvinylidene Fluoride Nanofibers for Enhancing Output Performance of Triboelectric Nanogenerators. *ACS Appl. Mater. Interfaces* **2020**, *12*, 17824–17832. [[CrossRef](#)]
11. Koç, M.; Paralı, L.; Şan, O. Fabrication and vibrational energy harvesting characterization of flexible piezoelectric nanogenerator (PEN) based on PVDF/PZT. *Polym. Test.* **2020**, *90*, 106695. [[CrossRef](#)]
12. Liu, W.; Thomopoulos, S.; Xia, Y. Nanofibers in Regenerative Medicine: Electrospun Nanofibers for Regenerative Medicine (Adv. Healthcare Mater. 1/2012). *Adv. Healthc. Mater.* **2012**, *1*, 2. [[CrossRef](#)]
13. Asran, A.S.; Henning, S.; Michler, G.H. Polyvinyl alcohol-collagen-hydroxyapatite biocomposite nanofibrous scaffold: Mimicking the key features of natural bone at the nanoscale level. *Polymer* **2010**, *51*, 868–876. [[CrossRef](#)]
14. Anu Bhushani, J.; Anandharamakrishnan, C. Electrospinning and electrospaying techniques: Potential food based applications. *Trends Food Sci. Technol.* **2014**, *38*, 21–33. [[CrossRef](#)]
15. Bhardwaj, N.; Kundu, S.C. Electrospinning: A fascinating fiber fabrication technique. *Biotechnol. Adv.* **2010**, *28*, 325–347. [[CrossRef](#)]
16. Sri Abirami Saraswathi, M.S.; Rana, D.; Divya, K.; Gowrishankar, S.; Nagendran, A. Versatility of hydrophilic and antifouling PVDF ultrafiltration membranes tailored with polyhexanide coated copper oxide nanoparticles. *Polym. Test.* **2020**, *84*, 106367. [[CrossRef](#)]
17. Fong, H. Electrospun nylon 6 nanofiber reinforced BIS-GMA/TEGDMA dental restorative composite resins. *Polymer* **2004**, *45*, 2427–2432. [[CrossRef](#)]
18. Kim, J.S.; Reneker, D.H. Mechanical properties of composites using ultrafine electrospun fibers. *Polym. Compos.* **1999**, *20*, 124–131. [[CrossRef](#)]
19. Jiang, S.; Chen, Y.; Duan, G.; Mei, C.; Greiner, A.; Agarwal, S. Electrospun nanofiber reinforced composites: A review. *Polym. Chem.* **2018**, *9*, 2685–2720. [[CrossRef](#)]
20. Luoh, R.; Hahn, H.T. Electrospun nanocomposite fiber mats as gas sensors. *Compos. Sci. Technol.* **2006**, *66*, 2436–2441. [[CrossRef](#)]
21. Chew, S.; Wen, Y.; Dzenis, Y.; Leong, K. The Role of Electrospinning in the Emerging Field of Nanomedicine. *Curr. Pharm. Des.* **2006**, *12*, 4751–4770. [[CrossRef](#)] [[PubMed](#)]
22. Pawłowska, S.; Rinoldi, C.; Nakielski, P.; Ziai, Y.; Urbanek, O.; Li, X.; Kowalewski, T.A.; Ding, B.; Pierini, F. Ultraviolet Light-Assisted Electrospinning of Core-Shell Fully Cross-Linked P(NIPAAm-co-NIPMAAm) Hydrogel-Based Nanofibers for Thermally Induced Drug Delivery Self-Regulation. *Adv. Mater. Interfaces* **2020**, *7*, 2000247. [[CrossRef](#)]
23. Burman, M.; Arinstein, A.; Zussman, E. Free flight of an oscillated string pendulum as a tool for the mechanical characterization of an individual polymer nanofiber. *Appl. Phys. Lett.* **2008**, *93*, 193118. [[CrossRef](#)]
24. Chou, S.-F.; Woodrow, K.A. Relationships between mechanical properties and drug release from electrospun fibers of PCL and PLGA blends. *J. Mech. Behav. Biomed. Mater.* **2017**, *65*, 724–733. [[CrossRef](#)]
25. Keun Kwon, I.; Kidoaki, S.; Matsuda, T. Electrospun nano- to microfiber fabrics made of biodegradable copolyesters: Structural characteristics, mechanical properties and cell adhesion potential. *Biomaterials* **2005**, *26*, 3929–3939. [[CrossRef](#)]
26. Andersson, R.L.; Ström, V.; Gedde, U.W.; Mallon, P.E.; Hedenqvist, M.S.; Olsson, R.T. Micromechanics of ultra-toughened electrospun PMMA/PEO fibres as revealed by in-situ tensile testing in an electron microscope. *Sci. Rep.* **2014**, *3*, 6335. [[CrossRef](#)]
27. Sukiman, M.S.; Andriyana, A.; Ang, B.C.; Metselaar, H.S.C. Elastic properties of electrospun PVDF nanofibrous membranes: Experimental investigation and numerical modelling using pixel-based finite element method. *Polym. Test.* **2020**, *81*, 106218. [[CrossRef](#)]
28. Mohammadian, M.; Haghi, A.K. Systematic parameter study for nano-fiber fabrication via electrospinning process. *Bulg. Chem. Commun.* **2014**, *46*, 545–555.

29. Haider, A.; Haider, S.; Kang, I.K. A comprehensive review summarizing the effect of electrospinning parameters and potential applications of nanofibers in biomedical and biotechnology. *Arab. J. Chem.* **2018**, *11*, 1165–1188. [[CrossRef](#)]
30. Huang, L.; Bui, N.-N.; Manickam, S.S.; McCutcheon, J.R. Controlling electrospun nanofiber morphology and mechanical properties using humidity. *J. Polym. Sci. Part B Polym. Phys.* **2011**, *49*, 1734–1744. [[CrossRef](#)]
31. Pelipenko, J.; Kristl, J.; Janković, B.; Baumgartner, S.; Kocbek, P. The impact of relative humidity during electrospinning on the morphology and mechanical properties of nanofibers. *Int. J. Pharm.* **2013**, *456*, 125–134. [[CrossRef](#)] [[PubMed](#)]
32. Szewczyk, P.K.; Gradys, A.; Kim, S.K.; Persano, L.; Marzec, M.; Kryshal, A.; Busolo, T.; Toncelli, A.; Pisignano, D.; Bernasik, A.; et al. Enhanced Piezoelectricity of Electrospun Polyvinylidene Fluoride Fibers for Energy Harvesting. *ACS Appl. Mater. Interfaces* **2020**, *12*, 13575–13583. [[CrossRef](#)]
33. Fashandi, H.; Karimi, M. Characterization of porosity of polystyrene fibers electrospun at humid atmosphere. *Thermochim. Acta* **2012**, *547*, 38–46. [[CrossRef](#)]
34. Li, W.W.; Qin, X.H. Effect of Relative Humidity on the Morphology of Electrospun Gelatin Aqueous Solutions. *Adv. Mater. Res.* **2014**, *941–944*, 1225–1228. [[CrossRef](#)]
35. Barua, B.; Saha, M.C. Influence of humidity, temperature, and annealing on microstructure and tensile properties of electrospun polyacrylonitrile nanofibers. *Polym. Eng. Sci.* **2018**, *58*, 998–1009. [[CrossRef](#)]
36. Peresin, M.S.; Habibi, Y.; Vesterinen, A.-H.; Rojas, O.J.; Pawlak, J.J.; Seppälä, J.V. Effect of Moisture on Electrospun Nanofiber Composites of Poly(vinyl alcohol) and Cellulose Nanocrystals. *Biomacromolecules* **2010**, *11*, 2471–2477. [[CrossRef](#)]
37. Venault, A.; Chang, Y.; Wang, D.-M.; Bouyer, D. A Review on Polymeric Membranes and Hydrogels Prepared by Vapor-Induced Phase Separation Process. *Polym. Rev.* **2013**, *53*, 568–626. [[CrossRef](#)]
38. Huang, C.; Thomas, N.L. Fabricating porous poly(lactic acid) fibres via electrospinning. *Eur. Polym. J.* **2018**, *99*, 464–476. [[CrossRef](#)]
39. Mohammadi, B.; Yousefi, A.A.; Bellah, S.M. Effect of tensile strain rate and elongation on crystalline structure and piezoelectric properties of PVDF thin films. *Polym. Test.* **2007**, *26*, 42–50. [[CrossRef](#)]
40. Bormashenko, Y.; Pogreb, R.; Stanevsky, O.; Bormashenko, E. Vibrational spectrum of PVDF and its interpretation. *Polym. Test.* **2004**, *23*, 791–796. [[CrossRef](#)]
41. Ma, H.; Yang, Y. Rheology, morphology and mechanical properties of compatibilized poly(vinylidene fluoride) (PVDF)/thermoplastic polyurethane (TPU) blends. *Polym. Test.* **2008**, *27*, 441–446. [[CrossRef](#)]
42. Szewczyk, P.K.; Metwally, S.; Karbowniczek, J.E.; Marzec, M.M.; Stodolak-Zych, E.; Gruszczynski, A.; Bernasik, A.; Stachewicz, U.; Stodolak-Zych, E.; Gruszczyn, A. Surface-Potential-Controlled Cell Proliferation and Collagen Mineralization on Electrospun Polyvinylidene Fluoride (PVDF) Fiber Scaffolds for Bone Regeneration. *ACS Biomater. Sci. Eng.* **2019**, *5*, 582–593. [[CrossRef](#)]
43. Viola, G.; Chang, J.; Maltby, T.; Steckler, F.; Jomaa, M.; Sun, J.; Edusei, J.; Zhang, D.; Vilches, A.; Gao, S.; et al. Bioinspired Multiresonant Acoustic Devices Based on Electrospun Piezoelectric Polymeric Nanofibers. *ACS Appl. Mater. Interfaces* **2020**, *12*, 34643–34657. [[CrossRef](#)] [[PubMed](#)]
44. Sezen, M.; Plank, H.; Fisslthaler, E.; Chernev, B.; Zankel, A.; Tchernychova, E.; Blümel, A.; List, E.J.W.; Grogger, W.; Pötl, P. An investigation on focused electron/ion beam induced degradation mechanisms of conjugated polymers. *Phys. Chem. Chem. Phys.* **2011**, *13*, 20235. [[CrossRef](#)]
45. Zaarour, B.; Zhu, L.; Huang, C.; Jin, X. Fabrication of a polyvinylidene fluoride cactus-like nanofiber through one-step electrospinning. *RSC Adv.* **2018**, *8*, 42353–42360. [[CrossRef](#)]
46. Wu, J.; Schultz, J.M.; Yeh, F.; Hsiao, B.S.; Chu, B. In-Situ Simultaneous Synchrotron Small- and Wide-Angle X-ray Scattering Measurement of Poly(vinylidene fluoride) Fibers under Deformation. *Macromolecules* **2000**, *33*, 1765–1777. [[CrossRef](#)]
47. Peterlin, A. Molecular model of drawing polyethylene and polypropylene. *J. Mater. Sci.* **1971**, *6*, 490–508. [[CrossRef](#)]
48. Murthy, N.S.; Grubb, D.T. Deformation of lamellar structures: Simultaneous small- and wide-angle X-ray scattering studies of polyamide-6. *J. Polym. Sci. Part B Polym. Phys.* **2002**, *40*, 691–705. [[CrossRef](#)]
49. Schultz, J.M. Microstructural aspects of failure in semicrystalline polymers. *Polym. Eng. Sci.* **1984**, *24*, 770–785. [[CrossRef](#)]
50. Park, J.H.; Rutledge, G.C. Ultrafine high performance polyethylene fibers. *J. Mater. Sci.* **2018**, *53*, 3049–3063. [[CrossRef](#)]

51. Arinstein, A.; Burman, M.; Gendelman, O.; Zussman, E. Effect of supramolecular structure on polymer nanofibre elasticity. *Nat. Nanotechnol.* **2007**, *2*, 59–62. [[CrossRef](#)]
52. Zhang, F.; Barber, A.H. Extreme Toughness Exhibited in Electrospun Polystyrene Fibers. *Macromol. Mater. Eng.* **2017**, *302*, 1700084. [[CrossRef](#)]
53. Stachewicz, U.; Bailey, R.J.; Wang, W.; Barber, A.H. Size dependent mechanical properties of electrospun polymer fibers from a composite structure. *Polymer* **2012**, *53*, 5132–5137. [[CrossRef](#)]
54. Richard-Lacroix, M.; Pellerin, C. Molecular Orientation in Electrospun Fibers: From Mats to Single Fibers. *Macromolecules* **2013**, *46*, 9473–9493. [[CrossRef](#)]
55. Lim, C.T.; Tan, E.P.S.S.; Ng, S.Y. Effects of crystalline morphology on the tensile properties of electrospun polymer nanofibers. *Appl. Phys. Lett.* **2008**, *92*, 141908. [[CrossRef](#)]
56. Papkov, D.; Zou, Y.; Andalib, M.N.; Goponenko, A.; Cheng, S.Z.D.; Dzenis, Y.A. Simultaneously Strong and Tough Ultrafine Continuous Nanofibers. *ACS Nano* **2013**, *7*, 3324–3331. [[CrossRef](#)] [[PubMed](#)]
57. Wu, C.-M.; Chou, M.-H.; Zeng, W.-Y. Piezoelectric Response of Aligned Electrospun Polyvinylidene Fluoride/Carbon Nanotube Nanofibrous Membranes. *Nanomaterials* **2018**, *8*, 420. [[CrossRef](#)]

Publisher’s Note: MDPI stays neutral with regard to jurisdictional claims in published maps and institutional affiliations.



© 2020 by the authors. Licensee MDPI, Basel, Switzerland. This article is an open access article distributed under the terms and conditions of the Creative Commons Attribution (CC BY) license (<http://creativecommons.org/licenses/by/4.0/>).